

Quasi-Elastic Scattering, Random Fields and phonon-coupling effects in $\text{PbMg}_{1/3}\text{Nb}_{2/3}\text{O}_3$

S N Gvasaliya^{1,3}, B Roessli¹, R A Cowley², P Hubert¹ and S G Lushnikov³

¹Laboratory for Neutron Scattering ETH Z & Paul Scherrer Institut, CH-5232 Villigen PSI, Switzerland

²Clarendon Laboratory, Oxford University, Parks Road, Oxford OX1 3PU, UK

³Lebedev Physical Technical Institute, 26 Politekhnicheskaya, 194021, St. Petersburg, Russia

Abstract. The low-energy part of the vibration spectrum in $\text{PbMg}_{1/3}\text{Nb}_{2/3}\text{O}_3$ (PMN) relaxor ferroelectric has been studied by neutron scattering above and below the Burns temperature, T_d . The transverse acoustic and the lowest transverse optic phonons are strongly coupled and we have obtained a model for this coupling. We observe that the lowest optic branch is always underdamped. A resolution-limited central peak and quasi-elastic scattering appear in the vicinity of the Burns temperature. It is shown that it is unlikely that the quasi-elastic scattering originates from the combined effects of coupling between TA and TO phonons with an increase of the damping of the TO phonon below T_d . The quasi-elastic scattering has a peak as a function of temperature close to the peak in the dielectric constant while the intensity of the central peak scattering increases strongly below this temperature. These results are discussed in terms of a random field model for relaxors.

PACS numbers: 77.80.-e, 61.12.-q, 63.50.+x, 64.60.-i

Submitted to: J. Phys.: Condens. Matter

1. Introduction

The family of complex perovskites $AB_{x_1}^0B_{1-x_1}^0O_3$ has been known for fifty years and are related to the classic ABO_3 perovskites but with different physical properties due to the chemical disorder on the B-sublattice. A very interesting sub-class of these complex perovskites is formed by the relaxor ferroelectrics, or shortly - relaxors. These materials have a frequency-dependent peak in the dielectric permittivity ϵ'' which typically extends over hundreds of degrees and is not directly related to any macroscopic changes of the symmetry. Since many physical properties of relaxors exhibit anomalies in this temperature range, the properties were called a "disuse phase transition". Despite many investigations, however, the nature of the disuse phase transition remains unclear [1, 2, 3, 4, 5].

PbMg_{1/3}Nb_{2/3}O₃ (PMN) is a model relaxor ferroelectric. It has the cubic Pm3m structure at all temperatures in the absence of an external electric field [6]. However, in an applied electric field, PMN undergoes a structural phase transition at $T_c \approx 210$ K [7] while the anomaly in the dielectric permittivity ϵ'' appears around the mean Curie temperature $T_m \approx 270$ K [1]. At a higher temperature, $T_d \approx 620$ K, the optical refractive index departs from the expected linear temperature dependence as observed by Burns and Scott [8]. This result was explained by the appearance of small polar regions of size of a few unit cells, which were referred to as 'polar nanoregions' (PNR).

The lattice dynamics of PMN and similar relaxor crystals PbMg_{1/3}Ta_{2/3}O₃ (PMT), PbZn_{1/3}Nb_{2/3}O₃ (PZN) and PbZn_{1/3}Nb_{2/3}O₃-xPbTiO₃ (PZN-xPT) has been studied by light [8, 9, 10, 11, 12, 13] and neutron scattering [14, 15, 16, 17, 18, 19, 20, 21, 22, 23, 24, 25, 26, 27, 28, 30]. First-order Raman light scattering was observed in both PMN and PZN [8], although first order scattering is forbidden if the crystal structure remains that of the cubic perovskites. Until now there is no detailed understanding for the origin of the apparent first order Raman scattering in the relaxors [12, 13]. The search for a soft mode by light scattering in PMN was unsuccessful [8, 12], whereas the results of neutron scattering measurements have lead to the suggestion that the soft TO phonons are overdamped for $q \approx 0.12 \text{ rlu}$ and $200 \text{ K} < T < T_d$ [16, 19, 21]. This anomalous behavior of the TO phonons was attributed to the formation of PNR in both PZN and PMN [17, 18, 19, 21], although an alternative interpretation was recently proposed that describes the results and the so called "waterfall" effect in terms of coupling between TA and highly damped TO phonons [24]. In addition, both light and neutron spectroscopy have reported a quasi-elastic (QE) component in the phonon spectrum of PMN [9, 11, 13, 27, 28, 30]. As anharmonicity is important in relaxors, it is a priori possible that this quasi-elastic mode originates from the strong coupling between the TA and heavily damped TO phonon modes [32].

In this work we have used high resolution neutron scattering to investigate the low-energy part of the vibration spectrum of PMN as described in section 2. We find in section 3 that the lowest transverse optic (TO) phonon branch is strongly coupled to the transverse acoustic branch (TA) above the Burns temperature, T_d , where the QE

component is absent. Below T_d , the results suggest that the phonon spectrum remains essentially unchanged, with the TO phonons found to be under-damped throughout the temperature range and the "waterfall effect" is not clearly observed at least in the $[0,0,q]$ direction. In addition there are two more components of the scattering consisting of a quasi-elastic, QE, component whose energy width is larger than the resolution and a central peak, CP, component whose energy width is the same as the resolution function. The energy and wave-vector width of the QE component have been measured and it is found that the QE susceptibility is a maximum at a temperature of about 370 K, a somewhat larger temperature than the maximum in the dielectric susceptibility. The CP component increases rapidly in intensity below 370 K similarly to the behaviour expected from an order parameter. The line-shape of the scattering as a function of wave-vector is not however a sharp Bragg reflection but is approximately a Lorentzian to the power of 1.5. In section 4 we shall suggest that these results are consistent with a random field model for this relaxor.

2. Experimental

The measurements were carried out with the three-axis spectrometer TASP, located at the neutron spallation source SINQ at the Paul Scherrer Institut, Switzerland. A high-quality single crystal of PMN ($\approx 8 \text{ cm}^3$) was mounted using a niobium holder inside a furnace. The measurements were performed in the temperature range 150 K – 670 K. The crystal was aligned in the (h, h, l) -scattering plane. The spectrometer had a pyrolytic graphite (PG) monochromator and analyzer and was operated in the constant final-energy mode. In the course of the measurements we had to search for compromises between the spectrometer resolution, the accessible (Q, ω) range, and the intensity. As a result several different spectrometer configurations were used. Most of data were collected in the following three configurations:

- (i) $k_f = 1.64 \text{ \AA}^{-1}$ and $10^\circ = \Delta \theta = 80^\circ \quad 80^\circ \quad 80^\circ$ collimation
- (ii) $k_f = 2.662 \text{ \AA}^{-1}$ and $10^\circ = \Delta \theta = 80^\circ \quad 80^\circ \quad 80^\circ$ collimation
- (iii) $k_f = 2.662 \text{ \AA}^{-1}$ and $10^\circ = \Delta \theta = 20^\circ \quad 20^\circ \quad 80^\circ$ collimation

where k_f refers to the energy of the scattered neutrons. In configuration (i) the $(0\ 0\ 2)$ Bragg reflection of PG was used for both the monochromator and analyzer, whereas the $(0\ 0\ 4)$ reflection was used for configurations (ii) and (iii). The energy resolution at zero energy transfer was 0.22 meV for configuration (i), 0.5 meV for (ii), and 0.25 meV for (iii), respectively. For configuration (i) the q -resolution along the scattering vector was $q_{\text{par}} = 0.015 \text{ \AA}^{-1}$ and $q_{\text{perp}} = 0.021 \text{ \AA}^{-1}$ in the transverse direction. For configurations (ii) and (iii) $q_{\text{par}} = 0.02 \text{ \AA}^{-1}$ and $q_{\text{perp}} = 0.04 \text{ \AA}^{-1}$, respectively. The vertical resolution was $q_z = 0.1 \text{ \AA}^{-1}$ with $k_f = 1.64 \text{ \AA}^{-1}$ and $q_z = 0.16 \text{ \AA}^{-1}$ with $k_f = 2.662 \text{ \AA}^{-1}$, respectively.

3. Experimental results and data analysis

3.1. Measurements above the Burns temperature at $T = 670$ K

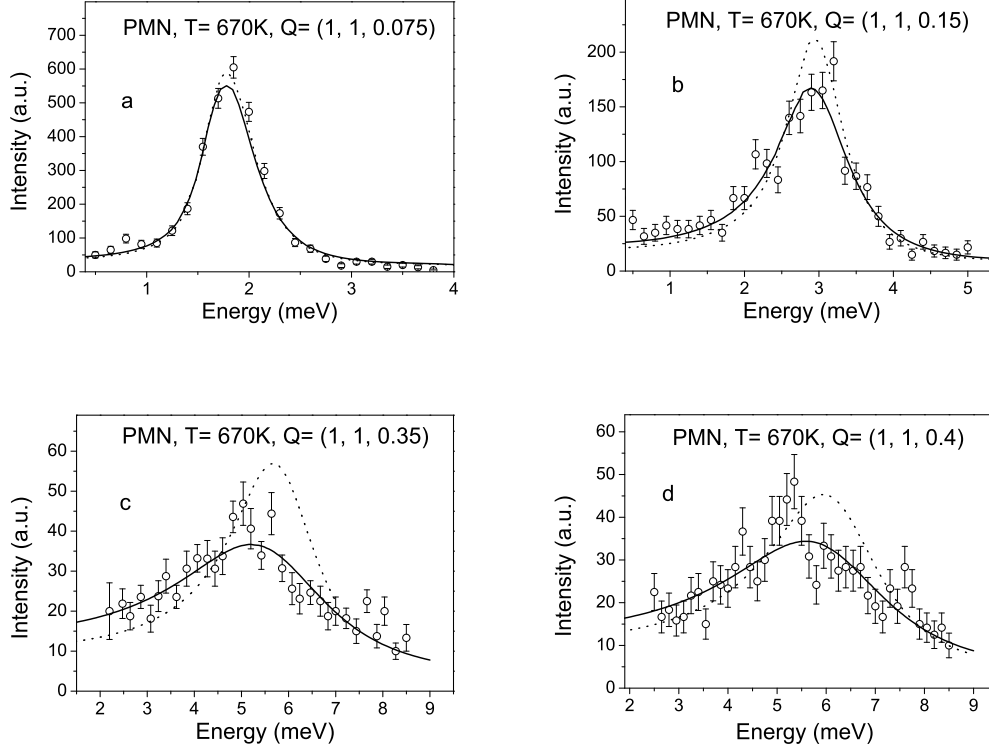


Figure 1. The results of typical constant- Q scans using configuration (i) in the $(1, 1, 0)$ BZ. The solid line shows the fit results whereas the dotted line corresponds to simulated spectra with the imaginary part of the coupling set to zero. See text for details. q is given in reciprocal lattice units (rlu). $1 \text{ rlu} = 1.55 \text{ \AA}^{-1}$.

The dynamical susceptibility for two coupled excitations was considered, for example in Refs. [31, 32, 33] and is given by

$$\chi_{CM}(\mathbf{Q}; \omega) = \frac{f_1^2 \chi_1 + f_2^2 \chi_2 + 2 f_1 f_2 \chi_{12}}{1 - \omega^2 - i \gamma}; \quad (1)$$

where $\chi_i = \chi_i(\mathbf{Q}; \omega)$, $i = 1, 2$ are the dynamical susceptibilities of the uncoupled phonons; and the f_i are the wave-vector dependent structure factors for the modes. The interaction term contains both real and imaginary parts and is assumed to have the simplified form: $\chi_{12} = (\chi_{12}^R + i \chi_{12}^I) \sin^2(\mathbf{q} \cdot \mathbf{r})$ where the q -dependence is chosen to be proportional to q^2 at small q as expected for a centrosymmetric crystal [31]. The dynamical susceptibilities of the TA and TO phonons are given by the damped-harmonic-oscillator functions (DHO):

$$\chi_{DHO}(\mathbf{q}; \omega) = \frac{(\chi_{q0}^2 - \chi_{q0} \omega^2 - \gamma^2)^{-1}}{1 - \omega^2 - i \gamma}; \quad (2)$$

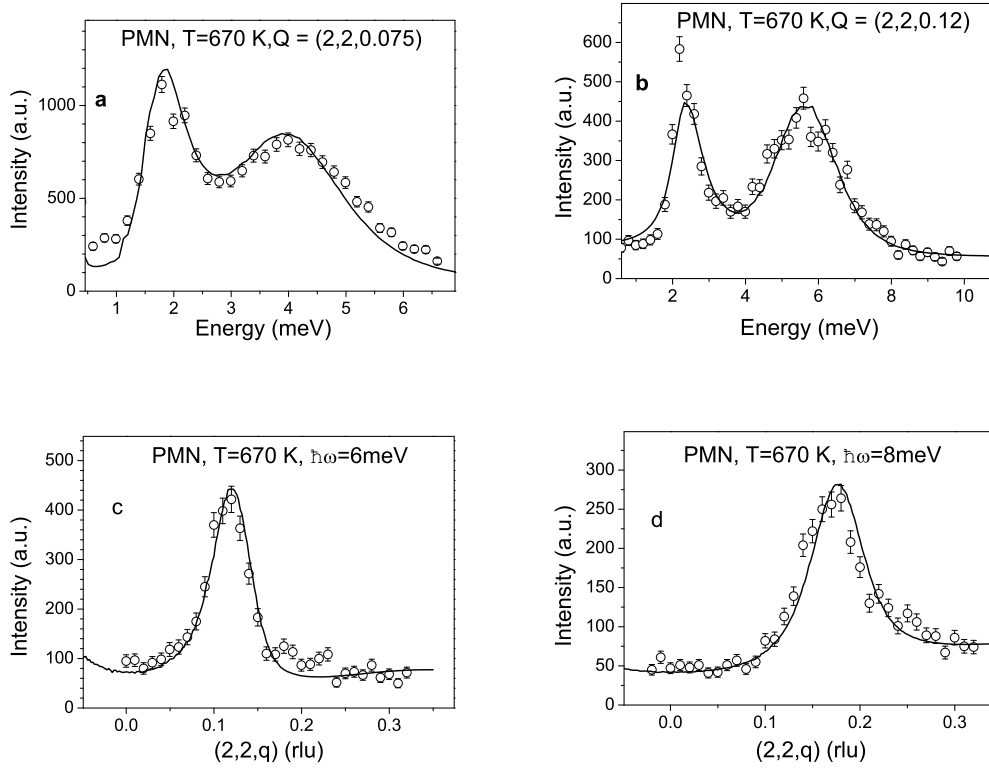


Figure 2. The results of typical constant-Q and with the results of constant-E scans taken in the (2,2,0) BZ using configuration (ii) with results of fits as explained in the text.

In Eq. 2, γ_q is the damping and ω_q is the renormalized frequency of a phonon.

When the damping is neglected the resonance frequency of the two coupled modes is given by:

$$\omega_{1,2}^2 = \frac{1}{2} (\omega_1^2 + \omega_2^2) \pm \frac{\gamma}{(\omega_1^2 - \omega_2^2)^2 + 4\gamma^2}; \quad (3)$$

where ω_1 and ω_2 are the frequencies of uncoupled excitations. To model the dispersion of the TA and TO phonons we have used the following parameterization based on a low q expansion

$$\omega_1 = \omega_{TA} = d \sin(q); \quad (4)$$

and

$$\omega_2^2 = \omega_{TO}^2 = \omega_{TO}^2(0) + c \sin^2(q); \quad (5)$$

The damping of TA phonon was found to increase with q approximately as

$$\gamma_{TA} = D_{TA} \sin^2(q); \quad (6)$$

and no assumption was made about the damping of the TO phonon.

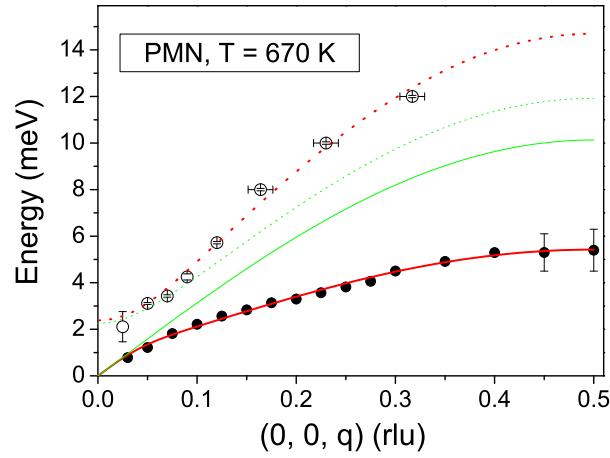


Figure 3. (Color online) Observed and calculated dispersion of the TA (solid circles) and the lowest TO (open circles) phonons in PMN along the $[00q]$ direction measured at $T = 670$ K. The solid and dotted green lines correspond to the calculated dispersion of the TA and TO phonons with coupling set to zero.

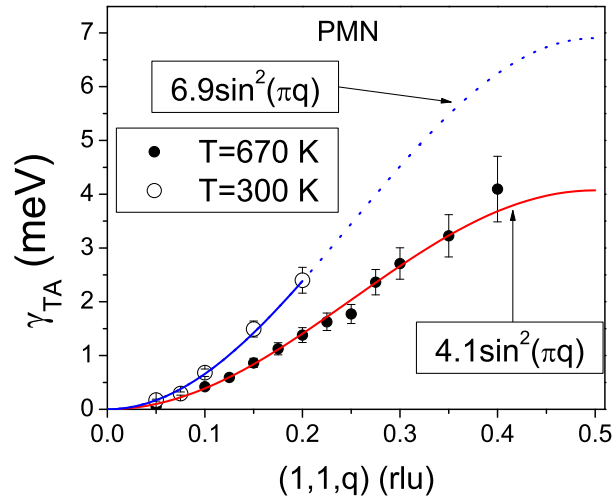


Figure 4. (Color online) q -dependence of the damping of the transverse acoustic phonon $T = 670$ K and $T = 300$ K (see text for details).

The neutron scattering intensity $I(\mathbf{Q}; \omega)$ was modelled as:

$$I(\mathbf{Q}; \omega) = S(\mathbf{Q}; \omega) \otimes R(\mathbf{Q}; \omega) + B \quad (7)$$

The symbol \otimes stands for the 4-D convolution with the spectrometer resolution function $R(\mathbf{Q}; \omega)$ [34], while B denotes the background level and $S(\mathbf{Q}; \omega)$ is the neutron scattering function which is related to the imaginary part of the dynamical susceptibility, $\chi''(\mathbf{Q}; \omega)$,

through

$$S(\mathbf{Q}; \omega) = \frac{[\hbar(\omega) + 1]}{\omega_{\text{CM}}} \omega_{\text{CM}}(\mathbf{Q}; \omega) \quad (8)$$

with the temperature factor $[\hbar(\omega) + 1] = [1 - \exp(-\hbar\omega/k_B T)]^{-1}$.

Figures 1 and 2 show typical inelastic neutron scattering spectra of PMN at $T = 670$ K in the $(1, 1, 0)$ and $(2, 2, 0)$ Brillouin zones (BZ) and the results of fitting these spectra to the interacting phonon model, Eq. 8. In the $(1, 1, 0)$ BZ only the TA phonon is observed in constant Q scans, whereas both TA and TO phonons are visible in the $(2, 2, 0)$ BZ. The values of parameters which correspond to the solid lines in Figs. 1 and 2 are: $d = 10.05 \pm 0.45$ meV, $D_{\text{TA}} = 4.1 \pm 0.5$ meV, $\omega_{\text{TO}}(0) = 2.1 \pm 0.2$ meV, $c = 137 \pm 9$ meV², $\omega_{12} = 85 \pm 7$ meV², $\omega_{12} = 1.5 \pm 0.5$ meV. The wavevector dependence of the damping of the TO phonon, γ_{TO} is given in Table 1. The TA and TO dispersion curves are correctly reproduced with this parameterization and the frequencies are shown in Fig. 3. Also shown in Fig. 3 is the dispersion of the TA and TO branches in the absence of coupling. The two branches do not cross and the dispersion of both branches is mostly affected by the coupling close to the zone boundary. As illustrated in Fig. 1 the imaginary part of the coupling affects the phonon line-shape mainly at large momentum transfers. Figure 4 shows that the damping of the TA phonon is proportional to $\sin^2(q)$ that was obtained from fitting the spectra individually. Finally, Fig. 5 shows the structure factor of the TA and TO modes.

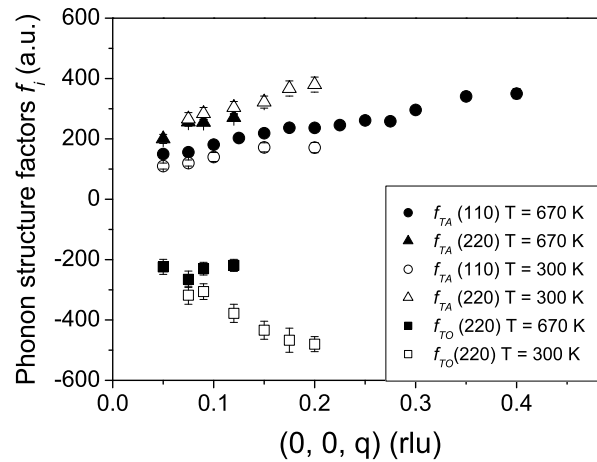


Figure 5. Wavevector dependence of the structure factors of the TA and TO phonons along the $[0, 0, q]$ direction.

3.2. Temperature dependence of the vibration spectrum

The energy and q space resolution was improved to study the temperature dependence of the TA and TO modes close to the Brillouin zone center. Figures 6 and 7 show

Table 1. Wave-vector dependence of τ_0 in PMN.

| q (rhu) | 0.05 | 0.075 | 0.09 | 0.12 | 0.15 | 0.175 | 0.2 |
|-----------------------|------|-------|------|------|------|-------|-----|
| τ_0 (670K) (meV) | 0.8 | 1.4 | 1.8 | 1.3 | — | — | — |
| Std. Error | 0.1 | 0.2 | 0.3 | 0.2 | — | — | — |
| τ_0 (300K) (meV) | 1.0 | 1.8 | 2.0 | 2.4 | 3.9 | 4.2 | 4.4 |
| Std. Error | 0.2 | 0.3 | 0.4 | 0.4 | 0.7 | 0.9 | 0.9 |

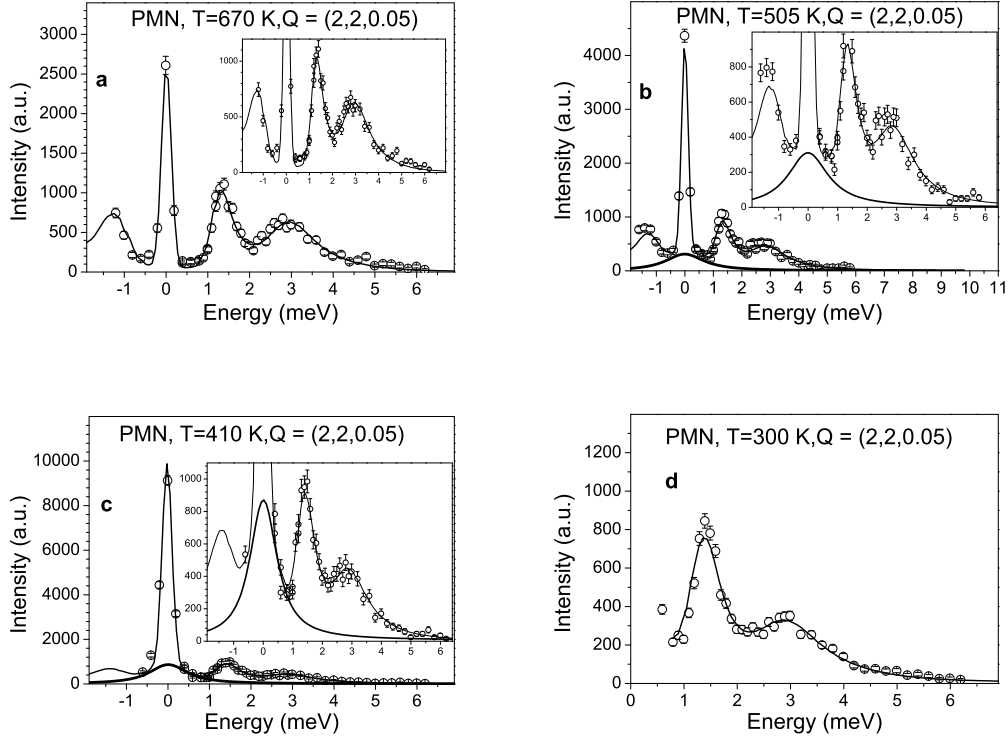


Figure 6. Observed and calculated spectra from constant- Q scans taken at $Q = (2, 2, 0.05)$ as a function of temperature. The contribution of $Q E$ scattering is shown by a bold solid line.

examples of spectra measured at $Q = (2; 2; 0.05)$ and $Q = (1; 1; 0.05)$, respectively. At 670 K, apart from the resolution limited elastic scattering, only scattering from the TA and TO phonons is observed. Upon decreasing the temperature, additional quasi-elastic scattering, $Q E$, becomes visible with an energy width larger than the resolution function while the more intense strictly elastic scattering, the CP component, increases on cooling especially below a temperature of 370 K. Both components of this elastic scattering have been observed previously in PMN [27, 28] and can be described by a resolution limited central peak (CP) and a Debye-like relaxation mode. The neutron-scattering susceptibility is given by:

$$S(Q; \omega) = S_{CP}(Q; \omega) \quad (9)$$

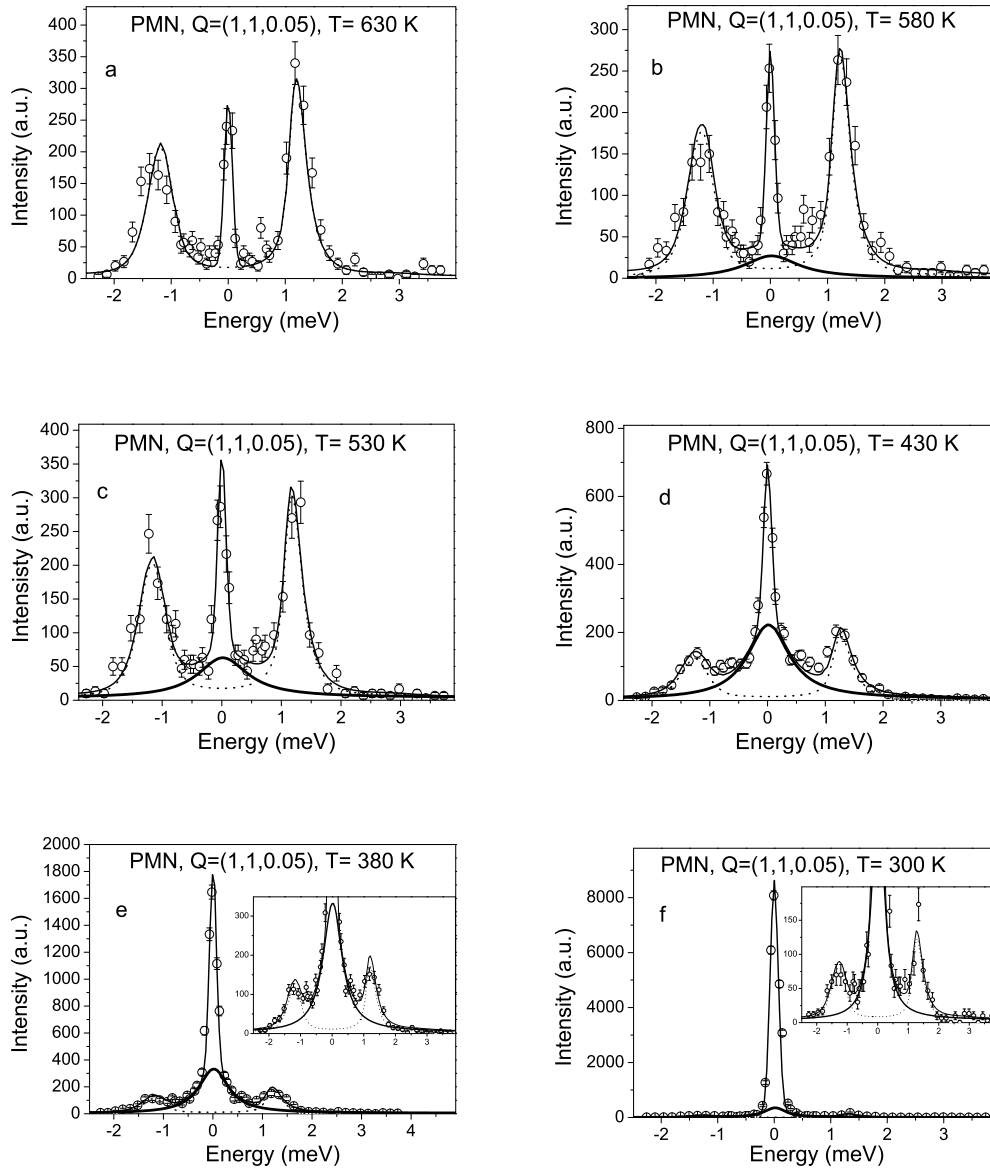


Figure 7. Observed and calculated spectra from constant- Q scans taken at $Q = (1, 1, 0.05)$. The contribution of QE scattering is shown by a bold solid line. Note the increase of CP intensity as the temperature is lowered below T_d . These measurements were performed using $k_f = 1.64 \text{ \AA}^{-1}$ and $10^\circ \times 20^\circ \times 20^\circ \times 80^\circ$ collimation.

$$+ \frac{[\hbar(\omega) + 1]}{2} [f_{CM}^2(Q; \omega) + f_{QE}^2(Q) f_{QE}^2(Q; \omega)];$$

$$S_{CP} = A(Q) \omega(\omega); \quad (10)$$

$$f_{QE}(q; \omega) = \frac{\omega(\omega)}{1 + q^2 \omega^2} \quad (1 - \omega^2 = q^2); \quad (11)$$

where $\delta(q)$ is the Dirac function; f_{QE} is the structure factor of the QE component and $\chi(q; T)$ is the susceptibility at $q = 0$; ξ is the correlation length of the QE scattering and $\chi(q) = \chi_0 + D_{QE} q^2$. S_{CP} describes the resolution-limited central peak with intensity $A(Q)$.

The model, described by Eqs. 7-11, was fitted to the neutron scattering at various temperatures and it gave good agreement with the results provided that the elastic scattering components were included. Typical results are shown in Figs. 6 and 7. In the temperature range between 300 K and 670 K for $q = 0.05$ rlu, the parameters describing the phonon line-shape remain essentially unchanged for this small wave-vector. However, the damping and the amplitude of the QE scattering change significantly as will be discussed in the next sub-section.

A more detailed measurement of the scattering as a function of wave-vector was performed with constant-Q scans around both the (1,1,0) and (2,2,0) BZ at $T = 300$ K. The results for the scattering and the fits to the model are shown in Figs. 8 and 9. We observe an increase of the damping of the TA and TO phonons and of the stiffness of the TO branch. The values of TA damping and TO stiffness at $T = 300$ K are $D_{TA} = 6.9 \pm 0.6$ meV and $c = 260 \pm 25$ meV²; the momentum dependence of the TO-phonon damping is summarized in Table 1. It is clear from the spectra shown in Fig. 9 and from Table 1 that at $T = 300$ K the lowest TO phonon is underdamped in the entire range of wave-vectors. Also the structure factors of the acoustic and optic branches do not change significantly with temperature as shown in Fig. 5.

The conclusion from this fitting is that although there is some temperature dependence of the phonon spectra at large wave-vectors q , at small wave vectors there is little temperature dependence and that we can essentially consider the low q high-energy phonons as temperature independent.

The constant-energy scans in PMN along $[2, 2, q]$ were measured to investigate the "waterfall effect" for $\sim \hbar\omega = 4, 6$ and 8 meV. The solid lines in Fig. 10 were obtained by varying only the intensities of the phonons and of the QE scattering while the other parameters of the phonons were fixed at the values obtained for $T = 300$ K. The model fits the experimental data very satisfactorily. We observe that the maxima in the spectra vary with the energy showing that the "waterfall" is not present at $T = 500$ K at least in (2, 2, 0) Brillouin zone.

3.3. Temperature dependence of the Elastic Scattering

The temperature dependence of the two components of the elastic scattering were also obtained from the fits of the model. Initially we shall consider the quasi-elastic scattering. The intensity of the quasi-elastic scattering is shown in Fig. 11. It increases on cooling below 600 K reaching a maximum at about 370 K and then decreases on further cooling. The frequency width of the scattering is shown in Fig. 12 as deduced from measurements with $q = 0.05$ rlu. It decreases with decreasing temperature from about 0.5 meV at 600 K to 0.1 meV at 200 K. The wave-vector dependence of the

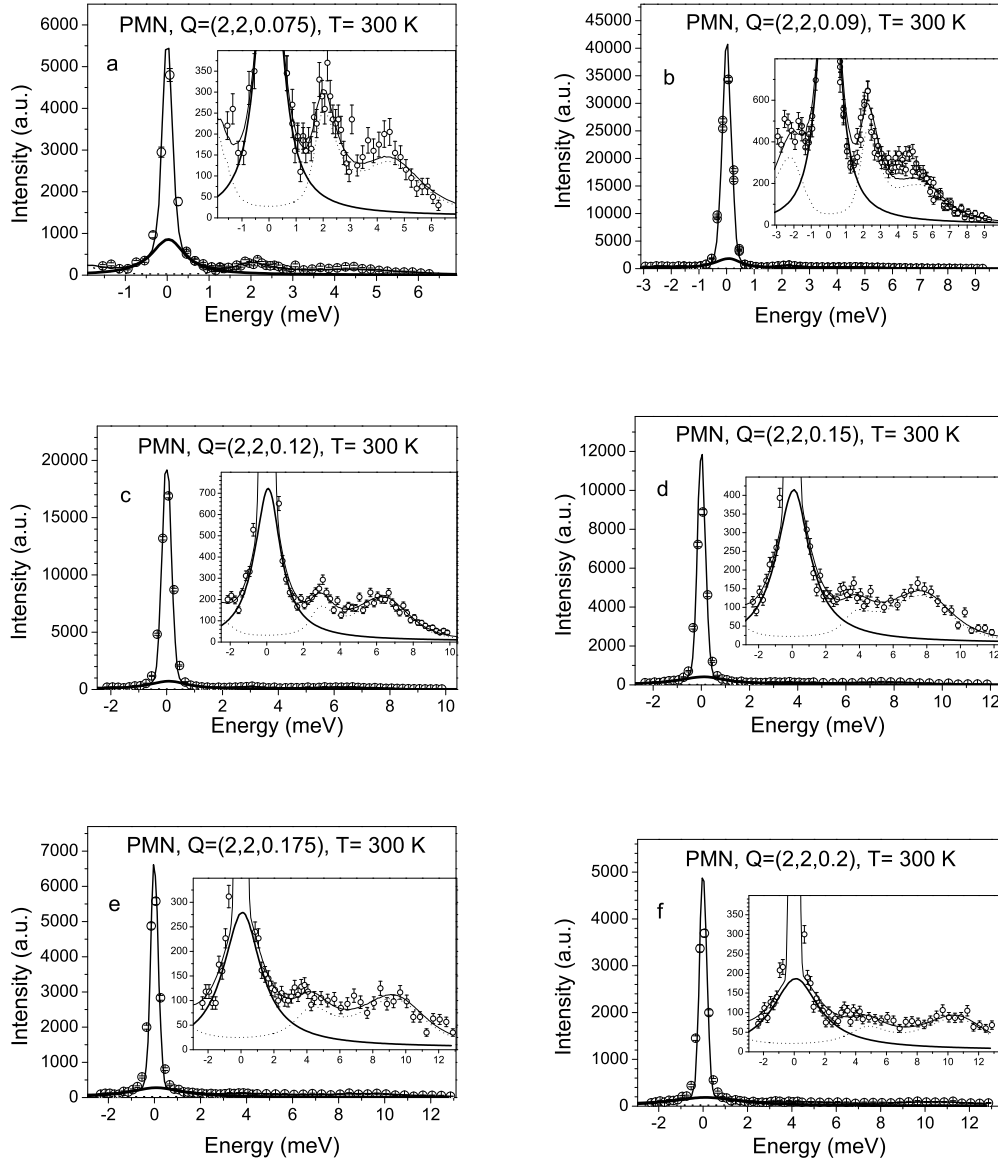


Figure 8. Observed and calculated spectra from constant- Q scans taken in the $(2,2,0)$ BZ at $T = 300$ K. Contribution of the QE component is emphasized by bold solid lines. The spectrum shown in Fig. 10a was measured with configuration (iii); other spectra were measured with configuration (ii).

width has been studied at temperatures of 450 K and 300 K and is shown in Fig. 13 for the latter temperature. It increases with wave-vector q and is at least approximately proportional to a constant and a quadratic term, as suggested above by Eqn. 11. The wave-vector dependence of the energy integrated intensity of the quasi-elastic component is also shown in Fig. 13 and it is consistent with a Lorentzian line shape, as suggested in Eqn. 11. The values of the parameters characterizing the QE scattering at the temperatures of 450 K and 300 K are $\Gamma = 7.2$ A and 11.2 A, $\Gamma_0 = 0.3 - 0.04$ meV

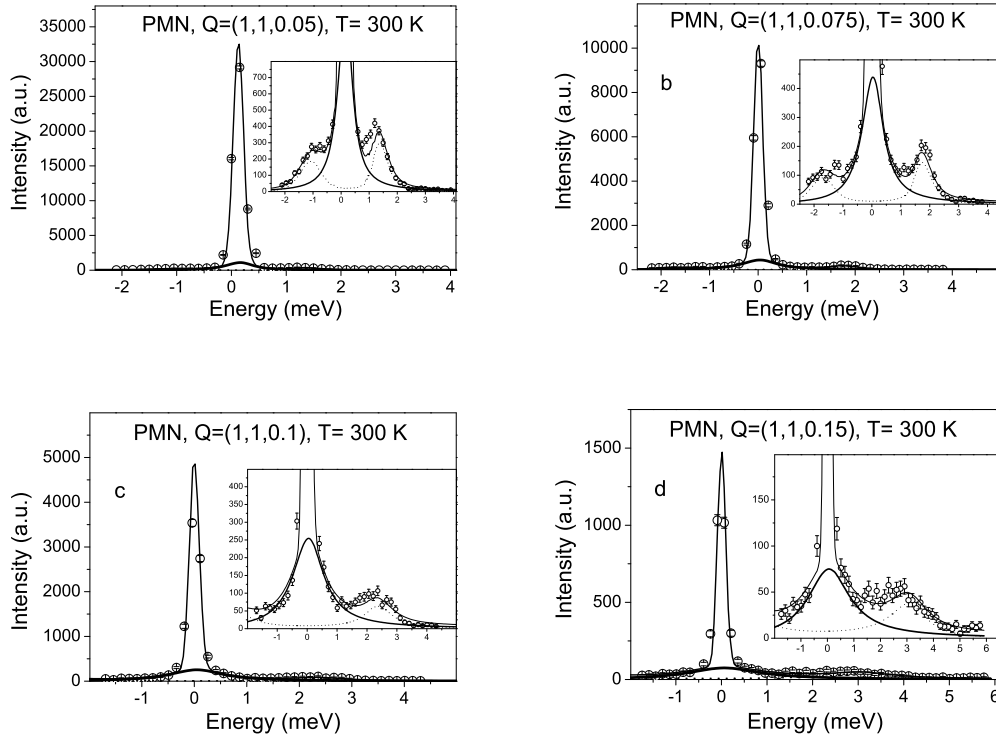


Figure 9. Observed and calculated spectra from constant- Q scans taken in the $(1,1,0)$ BZ and configuration (i). Contribution of the QE component is emphasized by bold solid lines.

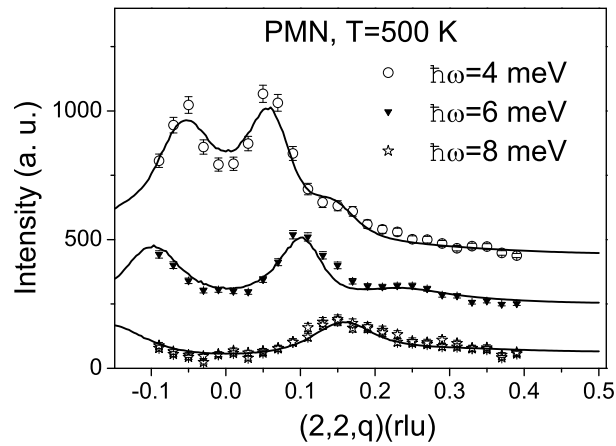


Figure 10. Constant-energy scans in PMN at $T = 500$ K. For means of comparison the scans have been shifted by 200 counts.

and 0.15 ± 0.03 meV while $D_{QE} = 19 \pm 2$ meV²Å² and 17 ± 2 meV²Å², respectively. The conclusion is that D_{QE} does not change as a function of temperature, within the

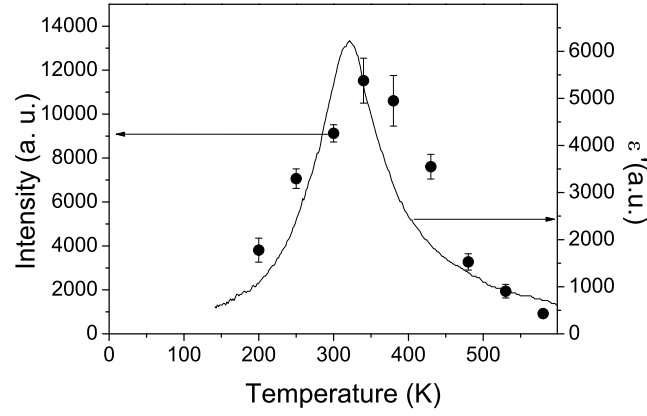


Figure 11. Temperature dependence of the susceptibility of the QE scattering in PMN measured at $Q = (1; 1; 0.05)$. For means of comparison the real part of the dielectric permittivity of PMN at frequency 1 GHz is also shown (Ref. [35]).

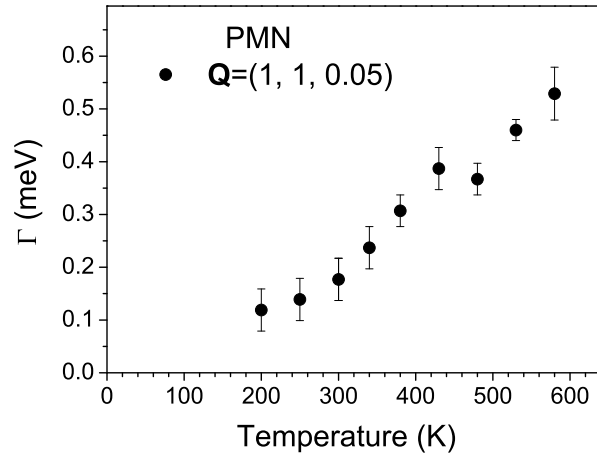


Figure 12. Temperature dependence of the damping of the QE scattering measured at $Q = (1; 1; 0.05)$.

precision of the measurements, but that the inverse correlation length and the damping at $q = 0$ both decrease as the temperature decreases and as illustrated for the inverse correlation length in Fig.14. Below 300 K, the correlation length remains approximately temperature independent but the damping still decreases.

The component of the central peak that is resolution limited is difficult to measure because it must be distinguished from the sharp and intense Bragg reflection on the one hand and from the incoherent scattering that is expected to vary only slowly with the wave-vector. Above about 480 K the intensity of the elastic scattering is weak

and away from the Bragg reflection it probably arises from the incoherent scattering. Below a temperature of 370 K the scattering rapidly increases in intensity as the sample is cooled as shown in Fig. 15. There appears to be some rounding possibly due to an inhomogeneous concentration distribution in the region of 370 K. The shape of the curve is nevertheless similar to that expected from an order parameter although in wave-vector it is wider than the Bragg reflection. The distribution of the intensity in wave-vector is determined by $A(Q)$. It is known e.g. from reference [20] that the distribution of the diffuse scattering in PMN is largely perpendicular to the wave-vector transfer. In Fig. 16 we show the measured intensity perpendicular to the $(1, 1, 0)$ Bragg reflection at 150 K, 300 K and 450 K. Clearly there is more diffuse scattering in the wings of the Bragg reflections at the two lower temperatures and in order to explain these results we have fitted the observations to the sum of a Bragg Gaussian, a flat background and a Lorentzian to an arbitrary power for the intermediate structure. As shown in Fig. 16 very reasonable descriptions were obtained when the intermediate peak was a Lorentzian to the power 1.5 while the inverse correlation function for this component slightly decreased from about 0.025(5) (rlu) at 300 K, to 0.015(5) (rlu) at 150 K. We note that at any temperature, the scattering by the central peak was found to be adequately described by a Lorentzian function to a power of about 1.5 and from our analysis of the data we conclude, that the correlation length decreases above room temperature to a value 0.04 (rlu) at 400 K.

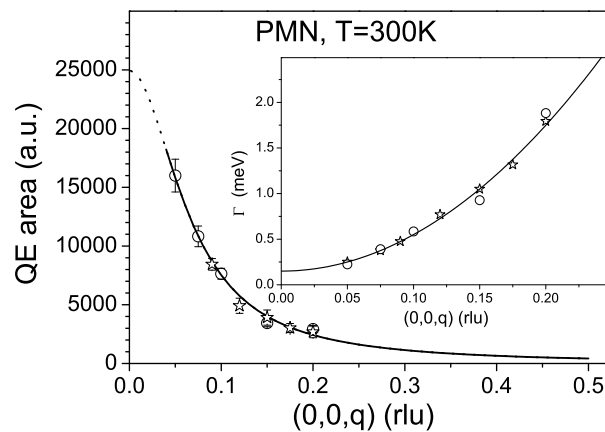


Figure 13. Wave-vector dependence of the energy-integrated intensity of the QE scattering in PMN measured in $(1, 1, 0)$ (circles) and $(2, 2, 0)$ (stars) Brillouin zones. Intensities of the QE component in two zones are scaled by a factor 1.3 at $q = 0.2$ rlu. The insert shows the q -dependence of the damping of the QE component; the error bars are within symbol size.

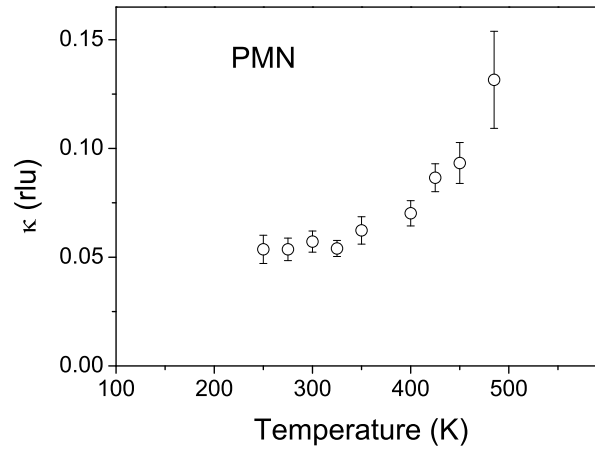


Figure 14. Temperature dependence of the inverse correlation length of the quasi-elastic scattering.

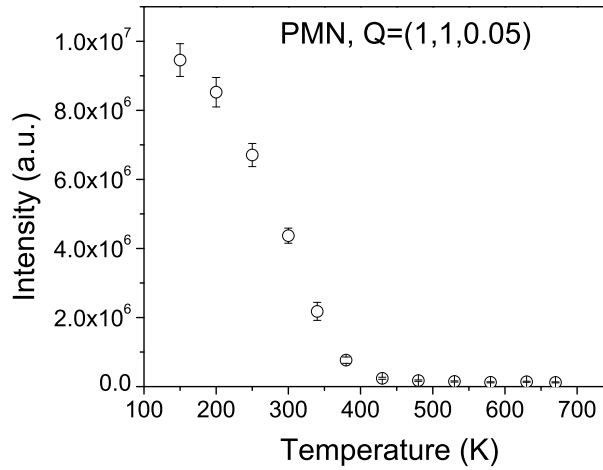


Figure 15. Temperature dependence of the intensity of the strictly elastic central peak.

4. Discussion and Conclusion

We have measured the low energy phonons in the relaxor ferroelectric PMN using high resolution neutron scattering techniques. Previously [18, 19, 20, 21] measurements were made of the neutron scattering in the (010) plane and using a more relaxed resolution function for the neutron scattering. Our results for the scattering in the (110) plane lead to quite a different picture and so initially we will compare and contrast our experimental results. The important phonons in PMN are the TA and lowest TO branches and we

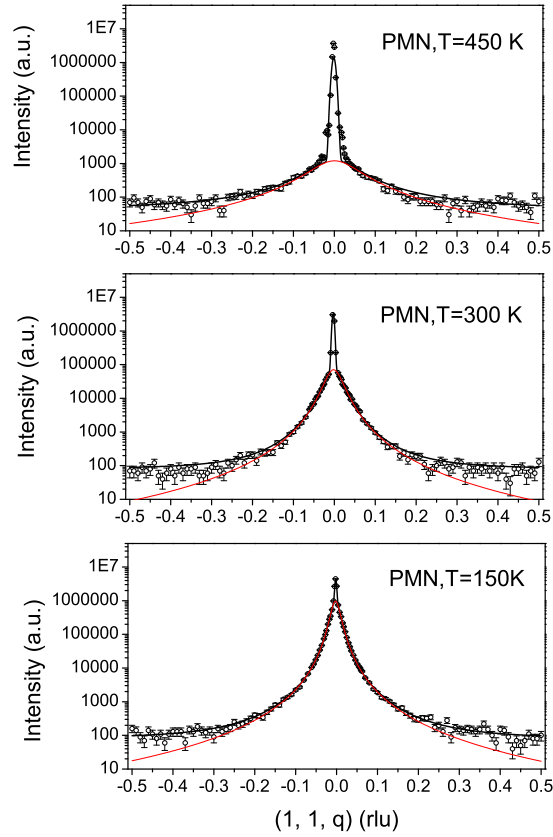


Figure 16. (Color online) Temperature dependence of the intensity of the elastic scans. These measurements were performed using $k_f = 1.4 \text{ \AA}^{-1}$ and $10^\circ = 20^\circ$ $20^\circ - 80^\circ$ collimation.

agree that there is a strong coupling between these two modes of vibration and that they can strongly interact because they have the same symmetry. The earlier work found that above the Burns temperature 620 K the TO mode was underdamped and decreased in frequency as the temperature was decreased. Below the Burns temperature it became overdamped and the frequency could not be obtained until the sample was cooled below a temperature of 200 K when it increased in frequency and became underdamped again. Throughout this intermediate region between 200 K and 620 K the TO mode exhibited the "waterfall effect" at which the mode has an infinite slope and the wave-vector is almost constant. The critical wave-vector 0.2 \AA^{-1} suggested that this behaviour results from the interaction of the mode with the polar nano-regions (PNR) and with the strong coupling between the mode and the TA modes. Later neutron scattering experiments [24] showed that the effect depends on the Brillouin zone and hence it is probably unlikely that it is due to the size of the PNR.

Our results differ in that throughout the region immediately below the Burns temperature we find that the inelastic scattering can be described at least at small wave-vectors in terms of largely temperature independent underdamped modes particularly for the TO mode. We also did not observe a "waterfall effect" for the TO mode. We consider that the reason for the first difference is that we used substantially better resolution than the previous work while for the second difference our observations were made in a different Brillouin zone and so our results support the conclusion of Hlinka et al. [24] based on their results for PZN.

The high resolution of our results did enable us to distinguish two components at low energies; one was the quasi-elastic scattering and the other the central peak. We have measured the intensity scattered by the TO mode and by the QE scattering and found that the ratio differs from one Brillouin zone to another. For example, the TO mode is weak near (110) above the TA mode but the QE scattering is present. The QE scattering might arise from the TO mode through the mode coupling because at low frequencies, below the TA phonon the TO mode would have a different eigenvector from that above the TA mode. We would then expect a different structure factor for the TO mode and the QE scattering as discussed in reference [20]. This effect does not however explain the difference in the intensities or the line shape of the scattering if the QE scattering is to be described by the interacting phonon model, outlined in the first part of section 3. We cannot however be certain that this is impossible if there is a strong frequency dependence to the self-energy of the TO mode, such as in the well known central peak problem in SrTiO_3 [36]. Nevertheless we shall in this paper discuss the QE scattering as though it was an independent mode of the crystal.

We observe that the quasi-elastic scattering appears below the Burns temperature T_d . Upon cooling the sample the susceptibility of the QE scattering increases rapidly and peaks around $T_m = 370 \text{ K}$. Simultaneously the characteristic time of the fluctuations increases. The frequency and wave-vector dependence of the scattering are strongly suggestive of a phase transition at that temperature. Thus we can conclude that below T_d we observe critical fluctuations that behave in a similar way to those of paraelectric or paramagnetic systems and one should expect a continuous phase transition when both the susceptibility and the correlation length diverge. The surprising feature is that the critical fluctuations in PMN have very low frequencies and are observed over an exceptionally wide temperature range between 200 K and 600 K. Most systems undergoing a phase transition have critical fluctuations that appear much closer to the phase transition and with much higher energies. This suggests that the fluctuations in PMN involve large collections of atoms, possibly PNR, rather than individual atoms. Below T_m the susceptibility of the critical fluctuations in PMN decrease while the correlation length is approximately temperature independent equal to 11 \AA^{-1} . This situation resembles the case of an antiferromagnet in a random-field.

The CP scattering is strictly elastic and so we shall assume that it is caused by short-range static displacements in which case it appears as diffuse scattering and not as Bragg scattering. The theory of the phase transition in an isotropic-three-

dimensional ferroelectric predicts that the critical fluctuations will be perpendicular to the wave-vector transfer. This scattering is then similar to that expected if the critical fluctuations of an isotropic ferroelectric were frozen in at a temperature somewhat above the phase transition. We observe that the intensity of the elastic diffuse scattering (EDF) increases strongly below $T = 370$ K expected for the temperature dependence of an order parameter. The FWHM of this scattering decreases below T_m indicating that static displacements are correlated over larger distances. The diffuse scattering, however, never turns into a Bragg reflection. Above T_m the diffuse scattering is very weak and disappears rapidly when approaching T_d in agreement with the results of Hiraka et al. [30]. Above T_m , the scattering is much weaker and it was difficult to analyse the line shape precisely, due to the presence of the strong Bragg peak. Below T_m , the line-shape of the diffuse scattering is described by a Lorentzian function raised to the power of $z = 1.5$. This is similar to the behaviour of an antiferromagnetic random field system in which the profile of the scattering is, after correction for the experimental resolution, a Lorentzian squared [37, 38]. If the correction is not made the observed profile depends on the detail of the resolution function but in some cases is observed to be a Lorentzian to the power of about 1.5. This onset of the elastic EDF scattering in PMN is very suggestive of a random field transition at 370 K at which the ferroelectric critical scattering becomes pinned by the random field associated with the atomic disorder or PNR.

It was suggested that the relaxors might be examples of random field transitions in reference [29]. However, a system with continuous symmetry is not expected to have a transition in the presence of a random field. Nevertheless PMN and other relaxors are cubic materials rather than being isotropic and the cubic symmetry breaks the continuous symmetry and allows for a random field transition. Most of the experimental work on random fields has been on random antiferromagnets in a uniform field which then generates a staggered antiferromagnetic field [37, 38]. The experimental results then show that it is possible to reach a number of meta-stable states when the sample is cooled in a field. In the case of relaxors there has been little theoretical work developing a random field theory and in particular on the form of the transition in a cubic material. We suggest that as the sample is cooled the atomic disorder gives rise to dynamic clusters of PNR, as occurs in PMN below the Burns temperature of 620 K. These do not order because the system is effectively isotropic at elevated temperature and fluctuations prevent the establishment of static order. At a temperature of about 370 K anisotropy starts to play a role and there is a cross-over to a cubic phase as opposed to an isotropic phase. The system then orders into a meta-stable random field phase that is stable down to the lowest temperature. The crystal reaches a uniform ferroelectric state if a large field is applied below a temperature of 210 K.

We are planning further experiments both to study the detailed shape of the ordering and to discover if we can observe any cross-over from isotropic to cubic symmetry as well as to study the QE scattering and the CP scattering in different Brillouin zones.

5. Acknowledgments

This work was performed at the spallation neutron source SINQ, Paul Scherrer Institut, Villigen (Switzerland) and was partially supported by RFBR grant 05-02-17822.

- [1] Smolenskii G A, Bokov V A, Isupov V A, Krainik N N, Pasynkov R E and Sokolov A I 1984 *Ferroelectrics and Related Materials* (New York: Gordon and Breach)
- [2] Cross L E 1987 *Ferroelectrics* 76 241
- [3] Westphal V, Kleemann W and Glushuk M D 1992 *Phys. Rev. Lett.* 68 847
- [4] Viehland D, Jang S J, Cross L E and Wuttig M 1992 *Phys. Rev. B* 46 8003
- [5] Blinc R, Dolinsek J, Gregorovic A, Zalar B, Filipic C, Kutnjak Z, Levstik A and Pirc R 1999 *Phys. Rev. Lett.* 83 424
- [6] de Mathan N, Husson E, Calvarin G, Gavarri J R, Hewat A R, Morell A 1991 *J. Phys.: Condens. Matter* 3 8159
- [7] Schmidt G, Amdt H, Vonnemann J, Petzsche T, Voigt H and Krainik N 1980 *Krist. und Tech.* 15 1415
- [8] Burns G and Scott B A 1973 *Solid State Commun.* 13 423
- [9] Lushnikov S G and Prokhorova S D 1989 *Ferroelectrics* 90 187
- [10] Laiho R, Lushnikov S G and Siny I G 1992 *Ferroelectrics* 125 493
- [11] Siny I G, Lushnikov S G, Katiyar R S and Rogacheva E A 1997 *Phys. Rev. B* 56 7962
- [12] Siny I G, Lushnikov S G, Katiyar R S and Schmidt V H 1999 *Ferroelectrics* 226 191
- [13] Svitelskiy O, Toulouse J, Yong G and Ye Z G 2003 *Phys. Rev. B* 68 104107
- [14] Naberezhnov A A, Vakhrushev S B, Dömer B, Strauch D and Moudou H 1999 *Eur. Phys. J. B* 11 13
- [15] Gehring P M, Park S E and Shirane G 2000 *Phys. Rev. Lett.* 84 5216
- [16] Gehring P M, Vakhrushev S B and Shirane G 2000 in *Fundamental Physics of Ferroelectrics 2000*, edited by R. E. Cohen (American Institute of Physics, Melville, NY), Vol. 535, p. 314.
- [17] Gehring P M, Park S E and Shirane G 2001 *Phys. Rev. B* 63 224109
- [18] Gehring P M, Wakimoto S, Ye Z G and Shirane G 2001 *Phys. Rev. Lett.* 87 277601
- [19] Wakimoto S, Stock C, Birgeneau R J, Ye Z G, Chen W, Buyers W J L, Gehring P M and Shirane G 2002 *Phys. Rev. B* 65 172105
- [20] Hirota K, Ye Z G, Wakimoto S, Gehring P M and Shirane G 2002 *Phys. Rev. B* 65 104105
- [21] Wakimoto S, Stock C, Ye Z G, Chen W, Gehring P M and Shirane G 2002 *Phys. Rev. B* 66 224102
- [22] Vakhrushev S B and Shapiro S M 2002 *Phys. Rev. B* 66 214101
- [23] Gvasaliya S N, Roessli B and Lushnikov S G 2003 *Europhys. Lett.* 63 303
- [24] Hlinka J, Kamba S, Petzelt J, Kulda J, Randall C A and Zhang S J 2003 *Phys. Rev. Lett.* 91 107602
- [25] Dömer B, Ivanov A S, Vakhrushev S B, Lushnikov S G, Gvasaliya S N, Strauch D and Schmalz K 2003 *Ferroelectrics* 282 9
- [26] Gvasaliya S N, Strauch D, Dömer B, Lushnikov S G and Vakhrushev S B 2003 *Ferroelectrics* 282 21
- [27] Gvasaliya S N, Lushnikov S G and Roessli B 2004 *Phys. Rev. B* 69 092105
- [28] Gvasaliya S N, Lushnikov S G, Roessli B 2004 *Cryst. Rep.* 49 108
- [29] Stock C, Birgeneau R J, Wakimoto S, Gardner J S, Chen W, Ye Z-G and Shirane G 2004 *Phys. Rev. B* 69 094104
- [30] Hiraka H, Lee S H, Gehring P M, Guangyong Xu and Shirane G 2004 *Phys. Rev. B* 70 184105
- [31] Coombs G J and Cowley R A 1973 *J. Phys. C* 6 121
- [32] Bruce A D and Cowley R A 1980 *Structural Phase Transitions* (London: Taylor and Francis)
- [33] Wehner R K and Steigmeier E F 1975 *RCA Review* 36 70
- [34] Popovich M 1975 *Acta Cryst. A* 31 507
- [35] Bovtun V, Kamba S, Pashkin A, Savinov M, Samoukhina P, Petzelt J, Bykov I P and Glushuk M D 2004 *Ferroelectrics* 298 23

- [36] Shapiro S M , Axe J D , Shirane G and Riste T 1972 Phys. Rev. B 6 4332
- [37] Yoshizawa H , Cowley R A , Shirane G and Birgeneau R J 1982 Phys Rev. Lett. 48 432
- [38] Cowley R A , Shirane G , Yoshizawa H , Uemura Y G and Birgeneau R J 1989 Z. Phys B - Condens. Matter. 75 303